Available online at www.sciencedirect.com

SciVerse ScienceDirect

Scripta Materialia 68 (2013) 579–582

Scripta MATERIALIA

www.elsevier.com/locate/scriptamat

Fracture toughness and toughening mechanisms in a (ZrB_2–SiC) composite reinforced with boron nitride nanotubes and boron nitride nanoplatelets

Chunguang Yue,[a] Weiwei Liu,[a] Lv Zhang,[a] Taihua Zhang[b] and Yao Chen[a,*]

[a]*School of Mechanical and Electric Engineering, Soochow University, 178 East Ganjiang Road, 215021 Suzhou, China*
[b]*The State Key Laboratory of Nonlinear Mechanics (LNM), Institute of Mechanics, Chinese Academy of Sciences, 15 Beisihuan Road, 100190 Beijing, China*

Received 5 October 2012; revised 5 December 2012; accepted 5 December 2012
Available online 12 December 2012

A ZrB_2–SiC composite reinforced with the mixture of boron nitride nanotubes (BNNTs) and boron nitride nanoplatelets (BNNPs) was prepared by spark plasma sintering. The results show that the fracture toughness of a (ZrB_2–SiC) composite increases by up to ~24.4% at 1.0% (BNNT–BNNP) weight fraction. The synergetic toughening mechanisms, including BNNT and BNNP pullout, crack bridging by BNNP, crack branching and crack deflection, and bending of multilayered BNNPs, are observed to contribute to the improved toughness.

Keywords: Ceramic matrix composites; Boron nitride nanotubes; Toughness; Spark plasma sintering

An ultrahigh-temperature ceramic composite, (ZrB_2–SiC) has attracted considerable attention because of its excellent combination of high melting point, high hardness and strength, good thermal stability, good oxidation resistance and corrosion resistance [1–3]. These properties make it a potential for ultrahigh-temperature aerospace applications, such as leading edge components in hypersonic and reusable launch vehicles, as well as high-temperature electrodes, nozzles and armors [4–6]. However, poor thermal shock resistance in the ZrB_2–SiC ceramic due to its low toughness is an obstacle that restricts its practical and potential applications [7].

Interest in enhancing the thermal shock resistance of (ZrB_2–SiC) has been sparked recently by two issues: further improvement in the fracture toughness of (ZrB_2–SiC) composites at room temperature [8] and reduction in the inner residual stress originating from the temperature gradient between different phases by the introduction of other phases with higher thermal conductivity into the (ZrB_2–SiC) composite [1]. Therefore, much effort has been devoted to developing novel (ZrB_2–SiC) composites that are reinforced with graphite flakes [8], ZrO_2 particles [9], carbon fibers [10] and carbon nanotubes [11]. Among these reinforcing materials, carbon nanotubes (CNTs) have been recognized as promising nanofillers due to the combination of outstanding mechanical properties and high thermal conductivity (~2980 W m^{-1} K^{-1}) [12]. Tian et al. [11] reported that the fracture toughness of a (ZrB_2–SiC) composite increases by up to ~15% at 2.0 wt.% CNTs. However, it is worth noting that the low starting oxidation temperature of CNTs (~400 °C) [13] might degrade the mechanical properties of CNT/(ZrB_2–SiC) composites at elevated temperatures.

As a structural analogue of CNTs, boron nitride nanotubes (BNNTs) have been proven to possess many good mechanical properties, such as high elastic modulus (~750–1200 GPa) [14,15] and tensile strength (>24 GPa) [16], which are comparable with those of CNTs [17]. Although the thermal conductivity of BNNTs (~600 W m^{-1} K^{-1}) [18] is much lower than that of CNTs, it is still nearly an order of magnitude higher than that of (ZrB_2–SiC) composites (50–140 W m^{-1} K^{-1}) [1], making it an effective way to enhance the thermal conductivity of (ZrB_2–SiC) composites. Furthermore, the higher starting oxidation temperature of BNNTs (~900 °C) [19] is also believed to guarantee less degradation of high-temperature performance of

* Corresponding author. Tel.: +86 521 6758 1872; fax: +86 512 6758 7216; e-mail: chenyao@suda.edu.cn

1359-6462/$ - see front matter © 2012 Acta Materialia Inc. Published by Elsevier Ltd. All rights reserved.
http://dx.doi.org/10.1016/j.scriptamat.2012.12.005

BNNT/(ZrB_2–SiC) composites. Previous investigations have revealed that the mechanical properties (including toughness and bending strength) of ceramics (i.e. HA [17], Al_2O_3 [20] and ZrO_2 [21]) improve greatly when reinforced with BNNTs. To the best of our knowledge, few investigations has been made into BNNT/(ZrB_2–SiC) composites.

Machining is of critical importance for the flexible use of the complex-shaped components of structural ceramics. In recent years, attempts have been made to improve the machinability of (ZrB_2–SiC) composites by introducing hexagonal boron nitride (h-BN) [22], which favors crack propagation and a decrease in cutting resistance during machining due to the cleavage plane of h-BN. Moreover, h-BN with low density, high thermal conductivity and chemical stability is also an attractive reinforcement to toughen (ZrB_2–SiC) composites [23].

The main aim of this study is to fabricate a (ZrB_2–SiC) composite reinforced with the mixture of BNNTs and h-BN nanoplatelets (BNNPs) using the spark plasma sintering (SPS) technique, and to investigate the synergetic effects of the additive (BNNT–BNNP) mixture on the fracture toughness of the (ZrB_2–SiC) composite.

Commercially available ZrB_2 powders with an average size of ~2 μm (Wuxi Yu Long Electronic materials Co. Ltd., China) and nanosized SiC particles (predominately α–SiC, purity >99%, Nanjing Emperor Nano Material Co. Ltd., China) with an average size of ~40 nm were selected as the starting precursors for the (ZrB_2–SiC) composite. The BNNTs–BNNPs mixture, in which the volume fraction of the BNNTs was ~40%, was purchased from Xian Feng Nano Material Co. Ltd., (Nanjing, China). As clearly depicted in Figure 1a, the as-received BNNTs are bamboo-like, with a diameter of ~50–400 nm and a length of ~1–2 μm, and the BNNPs are irregular platelets with a thickness ranging from ~50 to ~60 nm. The powders of ZrB_2 and 20 vol.% SiC were first mixed in ethanol using Si_3N_4 milling balls with a rotation rate of 300 rpm for 12 h. Then, 0.5 and 1.0 wt.% of (BNNTs–BNNPs), i.e. ~1.25 and ~2.49 vol.% of (BNNTs–BNNPs), were mixed with (ZrB_2–SiC) mixture in ethanol using Si_3N_4 milling balls with a rotation rate of 300 rpm for another 12 h. After being fully dried in an oven at 120 °C, the resulting powders were loaded into a graphite die (20 mm inner diameter), in which graphite papers were placed between the powders and die/punches for easy specimen removal. The mixed powders were sintered in an SPS apparatus (Dr. Sinter 1050, Sumitomo Coal Co. Ltd., Japan) with a holding temperature of 1550 °C and a holding pressure of 40 MPa. A heating rate of 150 °C min^{-1} was employed until 1450 °C was reached, with 1550 °C being attained in the next minute; this maximum temperature was then kept for 8 min. The samples were then cooled down to ambient temperature at the natural cooling rate of the furnace.

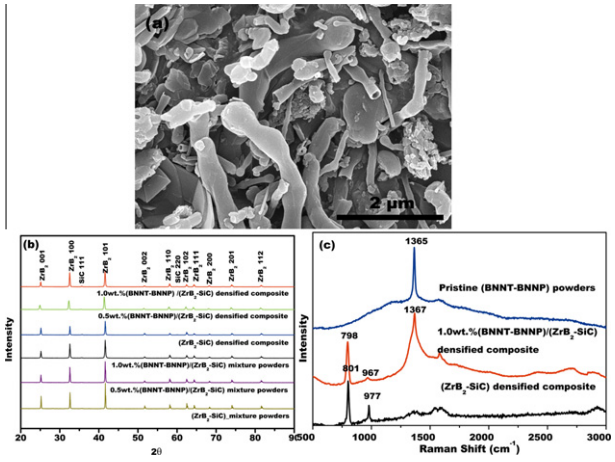

Figure 1. (a) SEM image of the as-received (BNNT–BNNP) mixture; (b) X-ray diffraction patterns of mixture powders and sintered composites; and (c) Raman spectra results of pristine (BNNT–BNNP), (ZrB_2–SiC) composite and 1.0 wt.%(BNNT–BNNP)/(ZrB_2–SiC) composite.

The bulk densities of the sintered samples were determined using Archimedes' method, while the relative densities were estimated by the rule of mixture. Phase constituents were analyzed by X-ray diffraction (XRD; X'Pert-Pro MPD, Holland) using Cu K_α radiation with a scanning rate of 0.5° min^{-1} and a scanning range of 20–90°. MicroRaman spectroscopy (JR HR800, France) was adopted to determine the existence of both BNNT and BNNP in the sintered composites using an argon ion laser with a wavelength of 514.5 nm and an acquisition time of 10 s. The elastic moduli (E) of the sintered samples were determined using an instrumented microindentation tester (CSM, Switzerland) with a Vickers tip. During the indentation, the load was applied up to a peak of 1000 mN in 30 s, then unloaded completely in 30 s after a dwell time of 15 s. The elastic modulus of the tested sample was calculated using Oliver–Pharr analysis [24]. The fracture toughness was evaluated using the following equation [25]:

$$K_{IC} = 0.016\left(\frac{E}{H}\right)^{1/2}\frac{P}{C^{3/2}} \quad (1)$$

where H is the Vickers hardness, E is the elastic modulus, P is the indentation load and $2C$ is the total length of indentation-induced crack $2C = 2l + 2a$, where l is the length of the crack from the indentation corner, and $2a$ is the indentation diagonal). Microhardness was measured using a microhardness tester (HXD-1000 TMC, Shanghai Taiming Optical Instrument Co. Ltd., Shanghai) with a Vickers probe and the application of a 4.9 N load applied for a dwell time of 15. At least 10 points were determined. The measurement of the modulus and fracture toughness enables us to compute the critical energy release rate using the following equation [26]:

$$G_{IC} = K_{IC}^2\left(\frac{1-v^2}{E}\right) \quad (2)$$

where G_{IC} is the critical energy release rate and v is the Poisson ratio, which is taken as 0.2 for ZrB_2-based composites. Fractographic observations of the sintered samples and the propagation paths of cracks induced by Vickers indentation were analyzed using scanning electron microscopy (SEM; Hitachi S-4700, Japan).

As clearly seen in Figure 1b, which shows the XRD patterns of the mixture powders and sintered samples,

the phases present in the samples are ZrB_2 and SiC. No peaks for either BNNTs or BNNPs are detected because of the low weight fraction of the (BNNT–BNNP) mixture incorporated into the composites. Raman spectra of the as-received (BNNT–BNNP) mixture and the sintered composites are shown in Figure 1c. This shows a characteristic peak of ~1367 cm^{-1}, confirming the existence of both BNNT and BNNP in the sintered composites. In addition, the characteristic peaks of SiC are also determined to be in the vicinities of ~798 and ~967 cm^{-1}. No peak for ZrB_2 is found due to its Raman inactivity [27].

Previous studies have reported that the relative densities of ceramic composites reinforced with CNTs or BNNTs decrease with increasing content of nanotubes [11,20]. However, the relative densities of the (ZrB_2–SiC) composites in the present study increase slightly with the addition of (BNNT–BNNP) mixture, as listed in Table 1. This is likely due to the existence of soft BNNPs. Both BNNTs and BNNPs at the grain boundaries might inhibit grain growth during SPS processing. In addition, BNNPs, with the capability of high-temperature ductile deformation, might fill in the contact gaps between grains under the high pressure applied during SPS, and subsequently decrease the size and quantities of the contact gaps between grains, in turn leading to increased densification.

Hardness is thought to be an important indicator for ceramic machinability, and a relatively lower hardness generally leads to improved machinability [22]. Compared to the (ZrB_2–SiC) composite, the additive (BNNTs–BNNPs) mixture has little effect on the Vickers hardness or the elastic modulus of the sintered composite (Table 1), implying that the (BNNT–BNNP) mixture does not adversely affect the machinability of the sintered (ZrB_2–SiC) composites. The good mechanical properties of BNNTs, i.e. an elastic modulus of ~750–1200 GPa [14–15] and a tensile strength of >24 GPa [16], are expected to increase the elastic modulus and hardness of the (ZrB_2–SiC) composite. On the other hand, BNNPs, with low hardness and low elastic modulus (~33.89 GPa in the *c* direction and ~85.95 GPa in the *a* direction) [28], are expected to decrease the hardness and the elastic modulus of the (ZrB_2–SiC) composite. Therefore, the synergetic effects of BNNTs and BNNPs could lead to minor changes in both the hardness and the elastic modulus of the (ZrB_2–SiC) composite. It is important to point out that, as listed in Table 1, the measured fracture toughness of the (ZrB_2–SiC) composite increases by up to 24.4% (from 3.73 ± 0.11 to 4.64 ± 0.36 MPa $m^{1/2}$) at 1.0% (BNNT–BNNP) weight fraction. Also, the critical energy release rate (G_{IC}), which quantifies the energy required to propagate the crack in the material, increases by up to 54.39% (from ~30.36 to ~46.87 J m^{-2}) when 1.0 wt.% (BNNT–BNNP) mixture is incorporated into the (ZrB_2–SiC). For CNT/(ZrB_2–SiC) composites, the enhancement in K_{IC} is ~15% at 2 wt.% CNT. These results strongly indicate that the (BNNT–BNNP) mixture is highly effective in suppressing crack propagation in the (ZrB_2–SiC) composite without degradation of its machinability.

To develop a comprehensive understanding of the contribution of the added (BNNT–BNNP) mixture to the improved toughness, the fractographic characteristics of the sintered samples were carefully analyzed using SEM. Figure 2a shows that BNNTs distribute uniformly in the composite, while the inset in Figure 2a shows that the BNNTs retain their original morphology after SPS processing. Figures 2b and 3c display the pullout of BNNTs and BNNPs. Both BNNT pullout and BNNP pullout can take effect during crack propagation and deflection, and dissipate energy due to binding and friction, subsequently leading to a toughened (ZrB_2–SiC) composite. It is evident from Figure 2d that bending

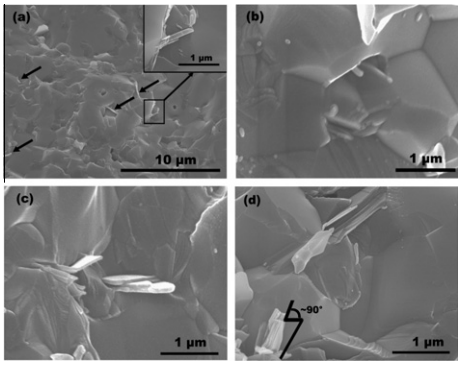

Figure 2. SEM photographs of fracture surfaces of 1.0 wt.% (BNNT–BNNP)/(ZrB_2–SiC) composite. (a) Uniform distribution of BNNTs in sintered composite (inset the BNNT with its original morphology), (b) BNNT pullout, (c) BNNP pullout and (d) multilayered h-BN bending.

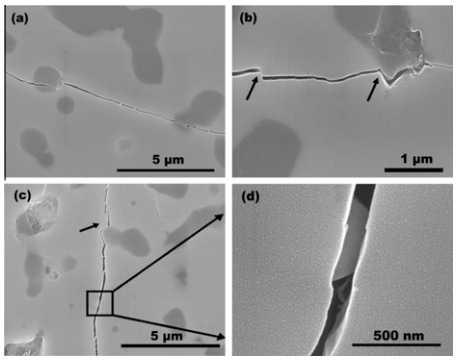

Figure 3. SEM micrographs showing indentation-induced cracks of (ZrB_2–SiC) (a), crack deflection (b), crack branching (c) and crack bridging by BNNP (d) of 1.0 wt.% (BNNT–BNNP)/(ZrB_2–SiC).

Table 1. Relative densities and mechanical properties of (ZrB_2–SiC) and (BNNT–BNNP)/(ZrB_2–SiC) composites.

Composites	Relative density (%)	E (GPa)	H (GPa)	K_{IC} (MPa $m^{1/2}$)	G_{IC} (J m^{-2})
(ZrB_2–SiC)	~98.62	440 ± 14	16.18 ± 0.63	3.73 ± 0.11	~30.36
0.5 wt.% (BNNT–BNNP)/(ZrB_2–SiC)	~98.71	445 ± 17	15.38 ± 0.85	4.33 ± 0.26	~40.45
1.0 wt.% (BNNT–BNNP)/(ZrB_2–SiC)	~98.75	441 ± 24	16.50 ± 1.38	4.64 ± 0.36	~46.87

of the multilayered BNNPs occurs on the fracture surface. This bending may originate from either applied pressure along with SPS or large deformation experienced during fracture. It is of significance that multilayered BNNPs without any fracture undergo such deformation that the bending angle approaches ~90° (Fig. 2d), leading to an L-shaped structure. When a crack propagates in the vicinity of the multilayered BNNPs, bending deformation might occur, thereby dissipating more energy. Subsequently, the stress concentration within the frontal process zone ahead of the crack tip reduces, slowing down and/or inhibiting crack propagation.

Figure 3 shows the crack propagation paths induced by Vickers indentation. As shown in Figure 3a, it is clearly seen that the crack advances in a straight line for the (ZrB_2–SiC) composite, and no obstacle is observed to inhibit the crack extension except the SiC phase. By comparison, the incorporation of (BNNT–BNNP) mixture into the (ZrB_2–SiC) composite causes the indentation-induced crack to propagate tortuously due to crack deflection (Fig. 3b). When a crack tip encounters a BNNT and/or a BNNP, it is deflected and absorbs some of the energy that is responsible for the crack propagation, resulting in a toughening of the matrix. Rafiee et al. [29] developed the classical Faber and Evans model [30] to illustrate that crack deflection is more effective for sheet-like reinforcement than for tubular-like reinforcement. Hence, it is expected that the addition of BNNPs contributes more to crack deflection than does the addition of BNNTs.

Crack branching is also observed as a toughening mechanism in the (BNNT–BNNP)/(ZrB_2–SiC) composite, with the length of secondary cracks being ~1 μm, as shown in Figure 3c. The phenomenon of crack bridging by BNNP is also visible in Figure 3d, which shows the plane of the BNNP to be nearly parallel to the polished surface. It is interesting to note that the bridged BNNP is found inside the crack (Fig. 3d); this can restrict the widening of the cracks, leading to more energy being required to open up the cracks. As a result, crack propagation is believed to be restricted when it approaches the vicinity of a BNNP.

In conclusion, (BNNT–BNNP)/(ZrB_2–SiC) composites fabricated by spark plasma sintering exhibit improved fracture toughness without any degradation of machinability. The fracture toughness of the (ZrB_2–SiC) composite increases by up to ~24.4% (from 3.73 ± 0.11 to 4.64 ± 0.36 MPa $m^{1/2}$) at 1.0% (BNNT–BNNP) weight fraction. The improvement in fracture toughness is likely due to the activated synergetic toughening mechanisms, such as BNNT and BNNP pullout, crack bridging by BNNP, crack branching and crack deflection. More interestingly, a novel toughening mechanism is observed that shows that bending of the multilayered BNNPs resists crack propagation through the dissipation of additional energy.

Y.C. acknowledges the financial support from the National Natural Science Foundation of China (Grant No. 51275326), the Natural Science Foundation of Jiangsu Province of China (Grant No. SBK2010212) and the Opening Fund of State Key Laboratory of Nonlinear Mechanics. T.H.Z. is grateful for financial support from the National Natural Science Foundation of China (Grant No. 11025212 and 11272318).

[1] S.Q. Guo, J. Eur. Ceram. Soc. 29 (2009) 995.
[2] W.J. Li, X.H. Zhang, C.Q. Hong, J.C. Han, W.B. Han, Mater. Sci. Eng. A 494 (2008) 229.
[3] Z. Wang, Z.J. Wu, G.D. Shi, Mater. Sci. Eng. A 528 (2011) 2870.
[4] X.H. Zhang, P. Zhou, P. Hu, W.B. Han, J. Eur. Ceram. Soc. 31 (2011) 2415.
[5] Q. Liu, W.B. Han, P. Hu, Scripta Mater. 61 (2009) 690.
[6] Z. Wang, S. Wang, X.H. Zhang, P. Hu, W.B. Han, C.Q. Hong, J. Alloys Compd. 484 (2009) 390.
[7] X.H. Zhang, Z. Wang, X. Sun, W.B. Han, C.Q. Hong, Mater. Lett. 62 (2008) 4360.
[8] X.H. Zhang, Z. Wang, P. Hu, W.B. Han, C.Q. Hong, Scripta Mater. 61 (2009) 809.
[9] D.J. Chen, W.J. Li, X.H. Zhang, P. Hu, J.C. Han, C.Q. Hong, W.B. Han, Mater. Chem. Phys. 116 (2009) 348.
[10] F.Y. Yang, X.H. Zhang, J.C. Han, S.Y. Du, J. Alloys Compd. 472 (2009) 395.
[11] W.B. Tian, Y.M. Kan, G.J. Zhang, P.L. Wang, Mater. Sci. Eng. A 487 (2008) 568.
[12] J. Che, W.A. Goddard, Nanotechnology 11 (2000) 65.
[13] M. Bertoncini, L.A.F. Coelho, I.O. Maciel, S.H. Pezzin, Mater. Res. 14 (2011) 380.
[14] N.G. Chopra, A. Zell, Solid State Commun. 105 (1998) 297.
[15] A.P. Suryavanshi, M.F. Yu, J. Wen, C. Tang, Y. Bando, Appl. Phys. Lett. 84 (2004) 2527.
[16] H.J. Shen, Comput. Mater. Sci. 47 (2009) 220.
[17] D. Lahiri, V. Singh, A.P. Benaduce, S. Seal, L. Kos, A. Agarwal, J. Mech. Behav. Biomed. 4 (2011) 44.
[18] M.R. Wang, Z.Y. Guo, Phys. Lett. A 374 (2010) 4312.
[19] Y. Chen, J. Zou, S.J. Campbel, G.L. Caer, Appl. Phys. Lett. 84 (2004) 2430.
[20] W.L. Wang, J.Q. Bi, S.R. Wang, K.N. Sun, M. Du, N.N. Long, Y.J. Bai, J. Eur. Ceram. Soc. 31 (2011) 2277.
[21] J.J. Xu, Y.J. Bai, W.L. Wang, S.R. Wang, F.D. Han, Y.X. Qi, J.Q. Bi, Mater. Sci. Eng. A 546 (2012) 301.
[22] H.T. Wu, W.G. Zhang, J. Eur. Ceram. Soc. 30 (2010) 1035.
[23] G. Li, W.B. Han, B.L. Wang, Mater. Des. 32 (2011) 401.
[24] W.C. Oliver, J. Mater. Res. 7 (1992) 1564.
[25] G.R. Anstis, P. Chantikul, B.R. Lawn, D.B. Marshall, J. Am. Ceram. Soc. 64 (1981) 533.
[26] M.A. Rafiee, J. Rafiee, I. Srivastava, Z. Wang, H. Song, Z.Z. Yu, N. Koratkar, Small 6 (2010) 179.
[27] D. Ghosh, G. Subhash, N. Orlovskaya, Acta Mater. 56 (2008) 5345.
[28] Z. Krstic, V.D. Krstic, J. Eur. Ceram. Soc. 28 (2008) 1723.
[29] M.A. Rafiee, J. Rafiee, I. Srivastava, Z. Wang, H.H. Song, Z.Z. Yu, N. Koratkar, Small 6 (2010) 179.
[30] K.T. Faber, A.G. Evans, Acta Metall. 31 (1983) 565.